scientific reports

Check for updates

OPEN

Molecular docking study and pharmacokinetic insights of rifampicin in pure and capsule dosage forms

Nahla A. Alassaf[1], Azhar S. Hamody[1], Majid S. Jabir[2]✉, Suresh Ghotekar[3] & Ayman A. Swelum[4]✉

To detect the amount of rifampicin in bulk and medicinal dosage formulations, an accurate and cost-effective UV spectrophotometric technique has been developed using the area under the peak to estimate the presence of rifampicin. This range of wavelengths (300–356 nm) was chosen. The method showed linearity in the 2–22 µg/mL range, with R^2 being^2 0.9996. The developed method's linearity, detection limit, quantification limit, precision, repeatability, and accuracy were all statistically and experimentally validated. The suggested methodology can be used for routine quality control analysis of rifampicin in pure form and in capsule dosage form, as demonstrated by the satisfactory recovery percentage results. This study explores the structural and electronic properties of rifampicin using density functional theory (DFT) and its interaction with potential biological targets via molecular docking. The DFT analysis, conducted using the B3LYP functional and a suitable basis set, provides detailed insights into the optimized molecular geometry, frontier molecular orbitals (FMOs), and molecular electrostatic potential (MEP) of rifampicin. The energy gap (ΔE = 2.878 eV) exported the stability conditions of rifampicin. Reduced density gradient analysis (RDG/NCI) was considered to highlight the specific interactions present inside the molecule, predicting its stability. Molecular docking studies complement the DFT analysis by identifying rifampicin binding affinity (-36.01 kcal/mol) with the specific 5F92 target protein. This study evaluates the ADMET properties of Rifampicin to assess its pharmacokinetic and safety profile.

Keywords Rifampicin, UV-spectroscopy, Density functional theory, Integrated DFT, Molecular Docking

Rifampicin, Fig. 1, {(2 S,12Z,14E,16 S,17 S,18R,19R,20R,21 S,22R,23 S,24E)- 5,6,9. ,17, 19-pentahydroxy-23-methoxy-2,4,12,16,18,20,22-heptamethyl-8-[[(4-methylpiperazin-1-yl) imino] methyl]-1,11 -dioxo-1,2-dihydro-2,7-(epoxypentadeca (1,11,13) trieneimino) naphtho[2,1-b] furan-21-yl acetate}, with content of (97.0-102.0) % as dry substance. Rifampicin is a brownish-red or brown crystalline powder, soluble in methanol but barely soluble in water, ethanol (96%) and in acetone[1]. It is considered an excellent antituberculosis agent against susceptible strains as well as ones resistant to isoniazid or streptomycin[2], and it is effective against a variety of diseases, including mycobacteria. Since its creation, it has been applied to the treatment of tuberculosis and other mycobacterial illnesses in both veterinary and human medicine[3].

The literature includes many research that deals with medical study[4–7] or analytical study[8] of rifampicin. Whether used alone or in conjunction with additional anti-tuberculosis medications in various pharmaceutical and in the body fluids, Rifampicin has been measured using a variety of techniques, including high-performance liquid chromatography[9–11], NMR spectroscopy[12], chemometrics techniques[13,14], chemiluminescence spectrometry[15], high performance thin layer chromatography[16], and LC-MS[17,18].

Several spectrophotometric methods have been developed, but all have been based on interaction of rifampicin with different chemical reagents or applying various chemometric methods. One of these methods[19]

[1]Department of Chemistry, College of Education for Pure Science/ Ibn Al-Haitham, University of Baghdad, Baghdad, Iraq. [2]College of applied sciences, university of technology, Baghdad, Iraq. [3]Centre for Herbal Pharmacology and Environmental Sustainability, Chettinad Hospital and Research Institute, Chettinad Academy of Research and Education, Kelambakkam 603103, Tamil Nadu, India. [4]Department of Animal Production, College of Food and Agriculture Sciences, King Saud University, Riyadh 11451, Saudi Arabia. ✉email: 100131@uotechnology.edu.iq; aswelum@ksu.edu.sa

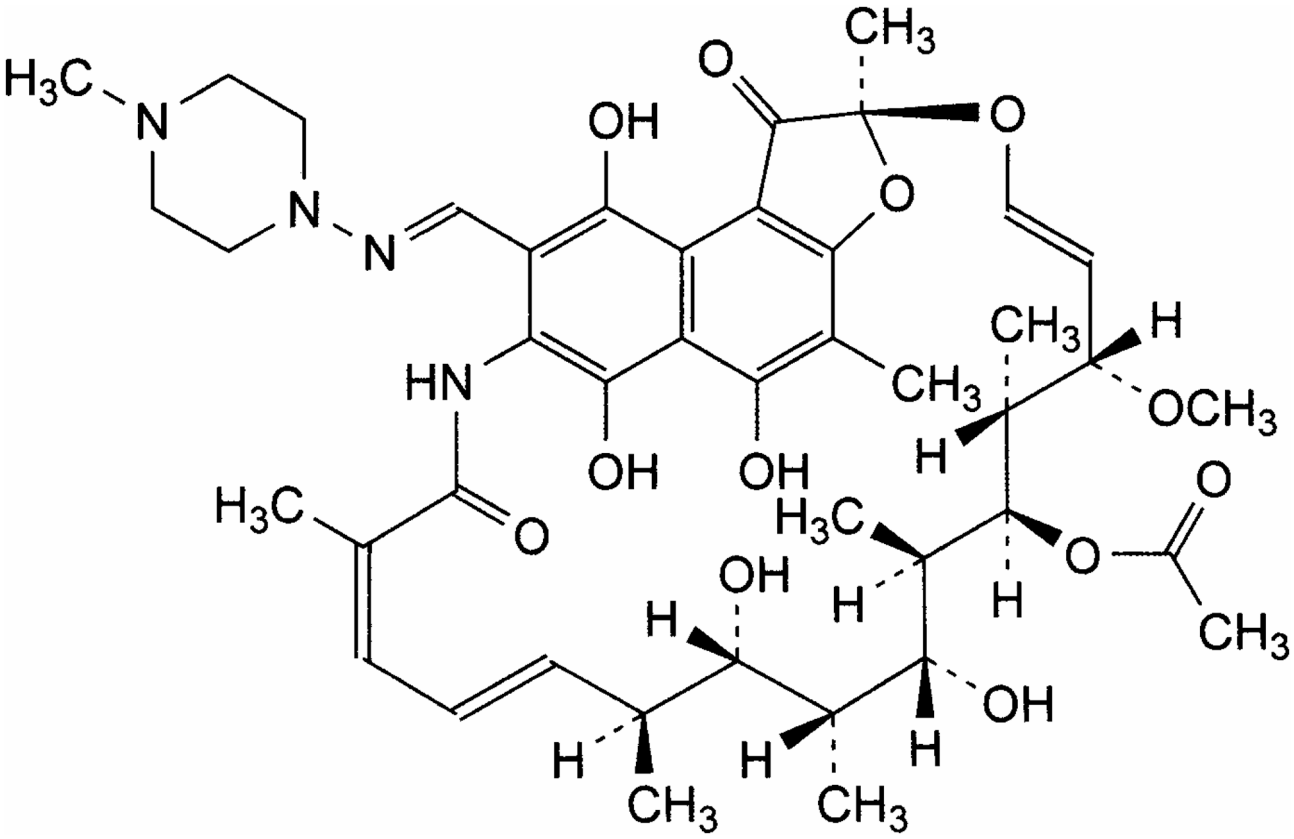

Fig. 1. Structure formula of Rifampicin.

involved the determination of rifampicin by reducing the Folin-Ciocalteu reagent by rifampicin to form a blue chromogen with λmax at 760 nm, as well as by reducing iron (III) by rifampicin in a neutral medium, and the resulting iron (II) is complexed with ferricyanide to form a Prussian blue peak at 750 nm. Another method[20] describe the estimation of rifampicin, isoniazid and pyrazinamide in their bulk and pharmaceutical dosage form by using first order derivative spectrophotometric method. Vierordt's method[21] was developed for the simultaneous determination of rifampicin and isoniazid with methanol, phosphate buffer pH 7.4 and citro-phosphate buffer pH 5.0 as solvents. UV spectrophotometry can be used in conjunction with multivariate calibration based on partial least squares regression for concurrent quantitative analysis of antibacterial mixture levofloxacin, metronidazole, rifampicin and sulfamethoxazole in their artificial mixtures and pharmaceutical formulations[22].

To overcome the urgent need to use chemicals that cause damage to the environment and because chemometric methods require special software and technical expertise in processing the results for all this area under peak method was developed in this study in an effort to create a straightforward, practical, and affordable UV spectrophotometric approach for determining rifampicin in bulk and pharmaceutical formulations. The developed method demonstrated high linearity, specificity, and accuracy for rifampicin and were assessed and validated in accordance with ICH[23] recommendations.

Materials and methods

Chemicals and reagents. All of the substances were of analytical quality, Rifampicin (≥ 97% (HPLC), powder) was supplied through Sigma-Aldrich-USA. Rifasynt 300 mg/capsule (Medochemie ltd/ Limassol, Cyprus) and RIFCAP 300 mg/capsule (Kocak Farma/Istanbul, Turky) were purchased from the local pharmacy.

Apparatus. All absorbance measurements were performed by using a Shimadzu UV-Visible spectrophotometer model 1800 (Kyoto, Japan) with matched quartz cells (1 mm).

Preparation of solutions. By dissolving 0.05 g of rifampicin in 50 mL of methanol, a standard stock solution of the drug (1000 µg/mL) was created. To create working stock solutions with concentrations of (100 and 50) µg/mL in the same solvent, additional dilution was made. A series of standard solutions with varying concentrations in the range of 2–22 µg/mL were made in a 5 mL calibrated volumetric flask. To validate the suggested methods and gauge the concentration of rifampicin, sample solutions of each of the two market brands (1000 µg/mL) were prepared.

DFT Methodology. To offer fully optimized geometrical and electronic calculations using the hybrid B3LYP approach, the designed heterocyclic Rifampicin molecule was submitted to a computational study using density functional theory (DFT)[24,25]. Gaussian 09 software was used to analyze the basis set 6-31G (d, p)[26], and MEP analysis was carried out to evaluate the important electrophilic and nucleophilic sites for the

optimized structures. Chemcraft[27] and VMD[28] software were used to analyze electronic behavior and display the heterocyclic compound's optimal structure and energy FMOs levels. Additional topological studies on reduced density gradient/non-covalent interaction (RDG/NCI) were carried out using Multiwfn software to demonstrate non covalent intermolecular and intramolecular interaction types[29]. MEP analysis was considered to describe the specific electronic density areas on the surface of the molecule.

ADMET technique and molecular docking. For very good outcomes, the docking process follows a critical path[30–32]. As a result, the AutoDock 4.2[33] program was used to simulate the docking of the complexes under investigation with control comparison. Additionally, docking data was analyzed and shown using Discovery Studio (https://www.3ds.com/products-services/biovia/). To conduct the in-silico study with potent support, Fumarate hydratase of Mycobacterium tuberculosis (ID:5F92) target protein was selected for this analysis[34]. The protein of interest was compared in a significant way on the Protein Data Bank website (https://www.rcsb.org/). After removing water molecules and any extraneous atoms from the target protein, the optimized heterocyclic compound was docked under particular conditions. The complexes were applied as pdbqt extension files after the protein charge was altered by the addition of polar H-atoms. The size of the grid box was determined, along with the expected active locations. The projected size of the grid box was 88 × 112 × 70 Å3 with grid centers' XYZ coordinates of 5.629, 10.478, and 39.775. The Genetic Algorithm (GA) was formerly thought to be the binding affinity method[35].

The bioavailability of bulk materials can be determined using Lipinski's rule of five, which is highly helpful for creating new medications[36]. With the help of the open-source ADMET-AI server (https://admet.ai.greenstonebio.com/) the ADMET parameters were determined and in silico tests of the Rifampicin drug-like characteristics were conducted.

Results and discussion

Area under peak analysis: The area under the peak is proportional to the total number of analyte molecules that have passed through the detector. It entails utilizing the formula[37]: Area under peak = $\int_{\lambda 1}^{\lambda 2} A\, d\lambda$, to calculate the integrated value of absorbance (A) with regard to the wavelength range between two chosen wavelengths (1 and 2). On the basis of repeated observation, the optimal wavelengths (1 and 2) for Rifampicin determination were chosen through fine scanning in the wavelength range 200–400 nm in diverse drug doses. Figure 2 illustrates the best wavelength selection, which was between 300 and 356 nm.

In absorption spectrum the unit of area under the peak is the product of the wavelength and absorbance units, so the result unit of the area is (absorbance-nm). As a result, the numerical magnitude of the peak area will never be the same as the peak height. A further drawback of measuring the area under a peak is that it requires pinpointing the peak's beginning and ending positions, which can be challenging, especially if there are several peaks that overlap[38].

Calibration plot. Ten solutions at different concentrations of Rifampicin (2, 3, 5, 7, 10, 13, 15, 17, 20, 22) µg/mL were prepared and measured at the pre-determined wavelength range 300–356 nm for area under peak analysis. The collected information was utilized to build the calibration curve. A good linear correlation was shown between the area under peak vs. concentration of Rifampicin as illustrated in Fig. 3. Because area is measured in different units, it is obvious that the slope has a higher numerical value for area under peak measurements.

For the assay of Rifampicin, in addition to linearity, values of LOD and LOQ were also calculated. Table 1 include the analytical parameters for the developed method.

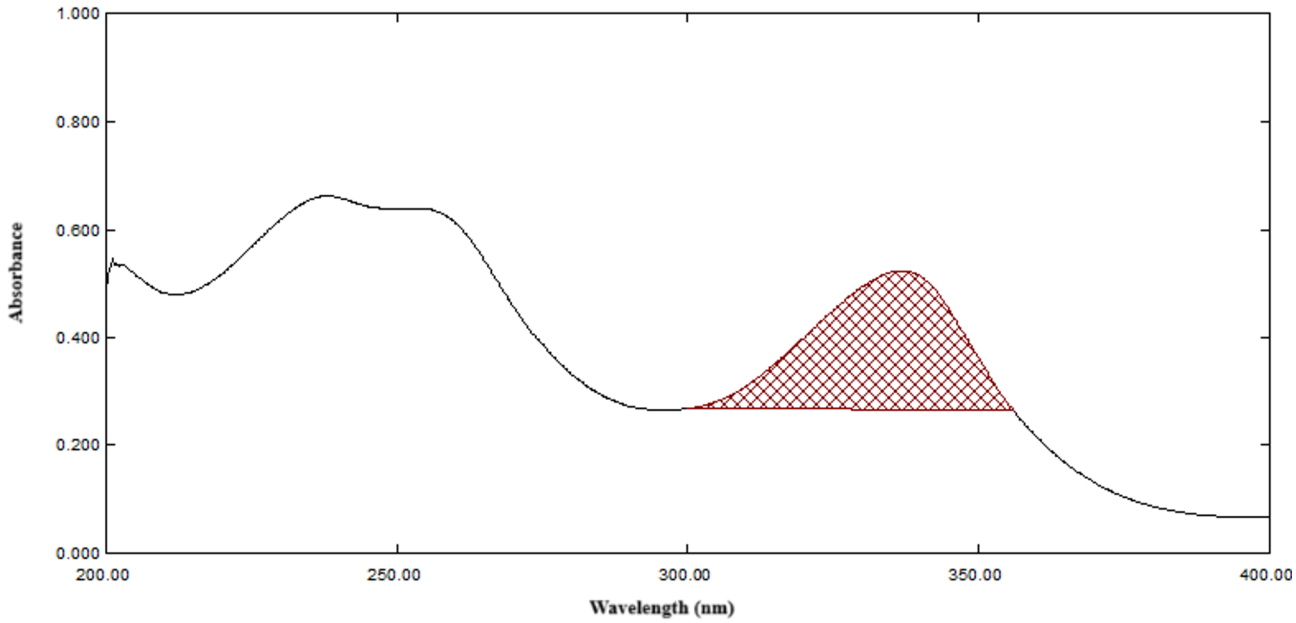

Fig. 2. Area under peak of 15 µg/mL of Rifampicin against the solvent blank.

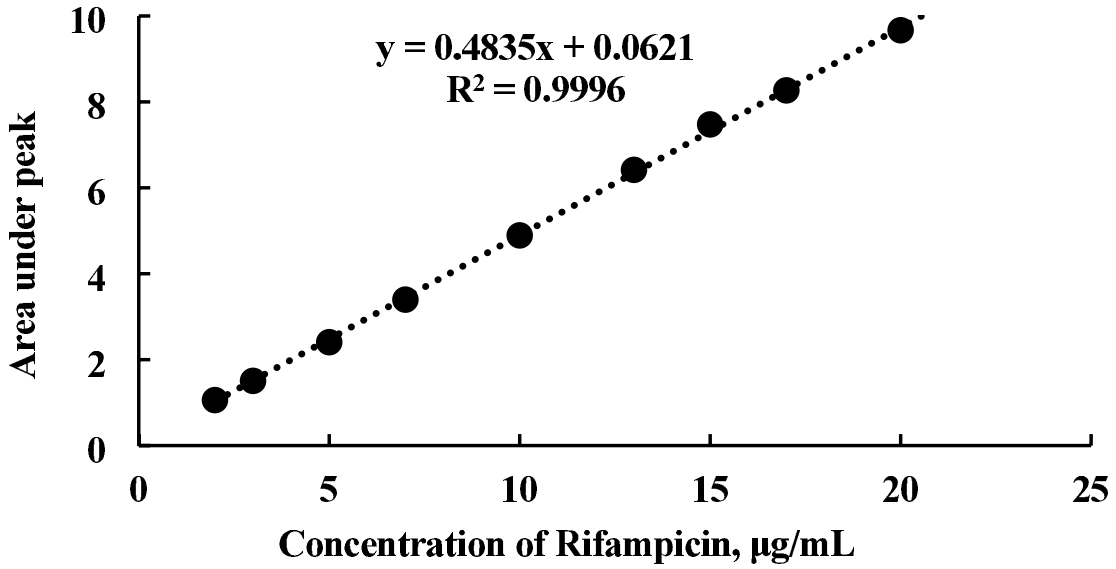

Fig. 3. Calibration plot of Rifampicin in the concentration range of 2–22 µg/mL versus area under peak.

Parameter	Variable
Wavelength	(300–356) nm
Range of linearity	(2.0–22.0) µg/mL
Regression formula	Area under peak = 0.4835[Rifampicin µg/mL] + 0.0621
Correlation coefficient (r)	0.9998
Calibration sensitivity	0.4835 mL/µg
Sandell's sensitivity	0.00207 µg/cm^2
Molar absorptivity	397920.5 L/mol.cm
LOD*	0.2855 µg/mL
LOQ*	0.8651 µg/mL

Table 1. Analytical parameters for the spectrophotometric determination of rifampicin via the developed method. * LOD = 3.3 (SD / slope),n = 9 measurements. * LOQ = 10 (SD / slope),n = 9 measurements.

In order to define the sensitivity features of the suggested method to determine Rifampicin in pharmaceutical formulations, the findings of the validation study were compared to other sensitive official methods, such as HPLC. Rifampicin concentration in human plasma was evaluated by Nada and co-authors using the HPLC technique at 337 nm in the concentration range of (0.3–25 µg/mL) in methanol as a solvent[10]. It is particularly encouraging to compare the validation outcomes of our study with spectrophotometric results obtained by Swamy and Basavaiah[19] employing redox and complexation reactions. They found that the LOD and LOQ for Rifampicin were 0.32 µg/mL and 0.96 µg/mL, respectively, the molar absorptivity was 2.72×10^4 L/mol.cm. and Sandell's sensitivity was 0.0302 g/cm^2.

Precision study. Intra-assay (repeatability) and intermediate precision[23] of the determination of Rifampicin via the proposed method was studied by calculating RSD% for five replicates at two concentration levels of Rifampicin. The results in Table 2 confirmed adequate drug stability and reliability for the suggested method where all the values of RSDs % were acceptable values.

Accuracy assay. This study was established by calculating of percentage of relative error of five replicates at two levels of Rifampicin concentration selected within the Beer's law limits. The analytical results found after the investigation are briefed in Table 2. The RE % values indicated that the proposed method have good accuracy.

Application of the proposed method in pharmaceutical samples. Commercially available capsules of Rifampicin were subjected to analysis by the proposed method. Figure 4 illustrate the area under beak for both pharmaceutical products Rifasynt, and RIFCAP respectively.

The quantitative determination of two concentration levels of the two market brands was carried out and the results, as illustrated in Table 3, were satisfactory. The good agreement between the taken and found concentrations of rifampicin in the capsules samples confirms the effectiveness of the proposed technique for

Intra-assay precision				Intermediate precision			
Concentration (µg/mL)				Concentration (µg/mL)			
Taken	Found*± SD	RSD %	RE%	Taken	Found*± SD	RSD %	RE%
5.00	4.79 ± 0.129	2.7	-4.200	10.00	9.75 ± 0.269	2.8	-2.454
7.00	6.72 ± 0.209	3.1	-4.070	15.00	15.02 ± 0.220	1.5	0.122

Table 2. Precision and accuracy for the determination of rifampicin by the proposed method. *Average of five measurements.

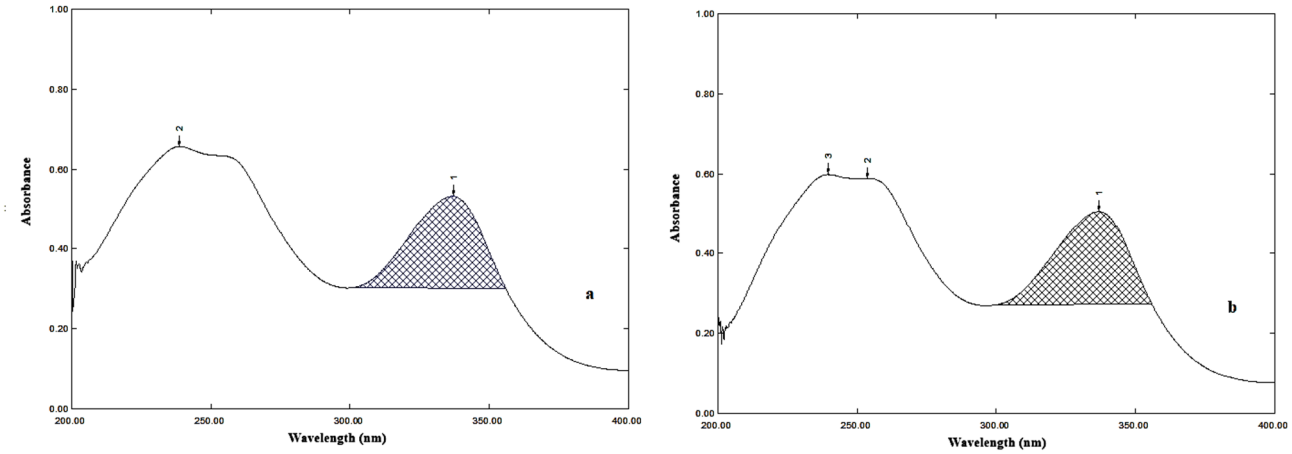

Fig. 4. Area under peak of 15 µg/mL of **a**: Rifasynt, **b**: RIFCAP against methanol as a blank.

Commercial sample	Amount* found (mg)	Concentration (µg/mL)		Recovery %	C.V. %
		Taken	Found*		
Rifasynt (Cyprus) 300 mg/capsule	285.227	10.000	9.46 ± 0.0457	94.55	0.483
	280.176	15.000	13.93 ± 0.0019	92.88	0.013
Rifcap (Turky) 300 mg/capsule	279.194	10.000	9.33 ± 0.0463	93.29	0.497
	275.452	15.000	13.81 ± 0.1383	92.05	1.002

Table 3. Quantitative content of rifampicin in pharmaceutical preparations determined via the proposed method. *Average of three measurements.

rifampicin quantification in pharmaceutical dosage forms. This consistency suggests that the method is both reliable and applicable for routine quality control.

*Geometrical structure and frontier molecular orbitals (FMOs)*Rifampicin has several aromatic moieties, such as naphthoquinone and other heterocyclic systems. It also involves several functional groups such as Hydroxyl (-OH), ketone (C = O), and amide groups that contribute to its interactions and geometry. Using the same theoretical level, Fig. 5 shows the geometrical structural convergence of the heterocyclic complex Rifampicin in the ground state under study. Bond lengths and bond angles are two crucial structural characteristics that can be discussed to better understand the conformational behavior of the structure in question. The highly heteroatomic-bearing compound exhibited a specific conformational structure in which the substituents were directed away from the carbon backbone of the compound. The bond angle values of the optimized structure enable the construction of the planarity behavior of the atoms. The bond lengths between C = O in different substituents (C2-O1, and C3-O3) were estimated with values of 1.228 Å and 1.23 Å. These results are based on variations in electronic environments. The values of C5-N2 double bond and N2-N3 single bond lengths are 1.294 Å and 1.361Å, respectively. H-bond formation is very important in the molecule to support several interactions. Intramolecular interactions of O4, O5, and N2 with the adjacent hydrogens are present with values 1.930, 2.168, and 2.290 Å, respectively. Bond angle values are mostly around 120°, C1-C2-O1and C4-C3-O3 angles were estimated with 121.64°, and 119.66°, respectively. Other bond angle values are displayed in Fig. 5c.

Studying the characteristics of compounds' frontier molecular orbitals (FMOs) is crucial for predicting the stability and reactivity of various molecules[39]. The most important molecular orbitals' energy distribution for the gaseous optimal structures are HOMO, and LUMO levels shown in Fig. 6. The value of the energy gap

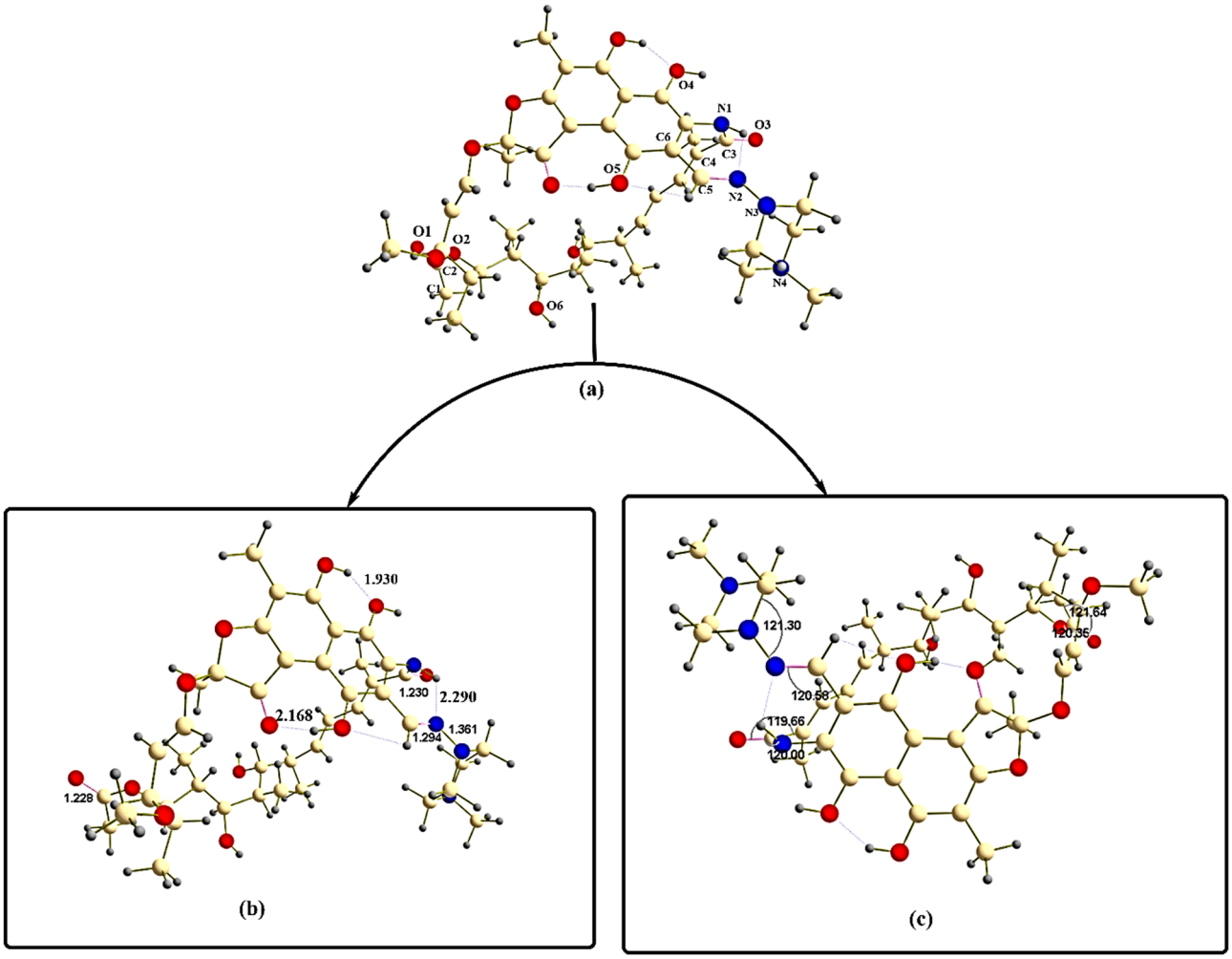

Fig. 5. The geometrical structure of the designed compound Rifampicin (a) labelled with, (b) bond lengths, (c) bond angles.

($\Delta E = 2.878$ eV, or 0.106 Ha) between HOMO and LUMO levels, a critical metric in the study of stability and reactivity, can be used to forecast the stability of the current heterocyclic complex[40]. The stability of both ground and excited states was further supported by the observation that the orbital contribution at all levels under investigation was mostly seen throughout the suggested molecule. The idea of consecutive donor-acceptor interactions in the excited states is brought about by the orbital contribution, which primarily occurs around the N atoms and OH groups.

The bond lengths shown in this study, such as the C = O bond at 1.228 Å, are indeed in good agreement with reported experimental and theoretical values. For instance, typical C = O bond lengths in esters and carbonyl compounds range from 1.20 to 1.23 Å, as found in both X-ray crystallographic data and computational studies.

Molecular electrostatic potential (MEP) The electronegativities of atomic positions on molecules are examined using the molecular electrostatic potential (MEP) 3D map. Since electrostatic forces are primarily responsible for long-range interactions, this topological index aids in the explanation of molecular contacts and recognition processes[41]. To find possible locations for electrophilic or nucleophilic attacks, the structure of the investigated compound was visually assessed using a color scale including red, orange, yellow, green, and blue (Fig. 7). Each atomic site's diminishing potential is represented by the color's orange, red, green, yellow, and blue. Consequently, an electron-rich site and an electron-deficient site are shown by red and blue zones, respectively. More specifically, it was anticipated that the examined compound's oxygen atom sites would all have the highest electronic richness, while the formed H-bond areas were potentially marked with blue color, indicating electron deficient areas. The remaining molecule parts would be working toward a neutral state.

Reduced density gradient/non-covalent-interactions (RDG/NCI) Several molecular locations were shown to have noncovalent bond interactions (NCIs) using reduced density gradient (RDG) research. The various noncovalent interactions were depicted using different color codes[42]. Repulsion (steric) interactions, which have a red color scale, and vdW interactions, which have a green color scale, are the two types of interactions that are easily visible on the surface of each molecule, as seen in Fig. 8. The intensity of the HB interaction in compounds is shown by the sign $(\lambda_2)\rho$, which is produced by multiplying the electron density by the sign of the second

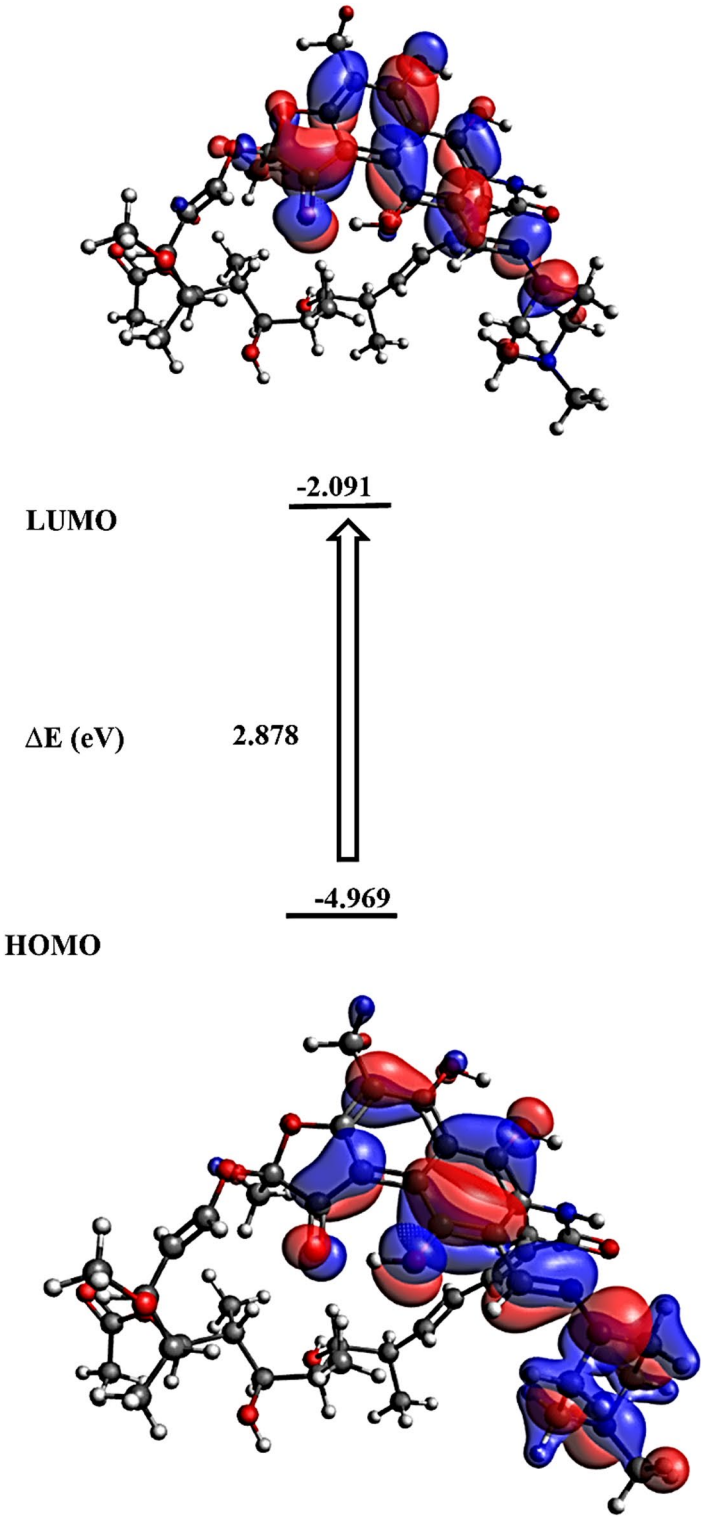

Fig. 6. FMOs levels with energy values (eV) of Rifampicin.

Hessian eigenvalue. VdW is easily discernible in the cages of the phenyl rings and increases near the methyl groups. The presence of H-bond blue spikes added extra stability to the molecular structure, which is distributed in several areas on the surface. The steric effect of phenyl rings, which enclose a 6-atomic system, restricts behaviour, was identified as the cause of the molecule's adverse repelling forces. The existence of advantages of H-bonds and electrostatic contacts can eliminate this kind of steric interaction.

Molecular Docking analysis: In-silico docking prediction can be used to study the bioactive behavior of the proposed system[43]. To assess the optimal docked complex, the investigated structure was immersed in the

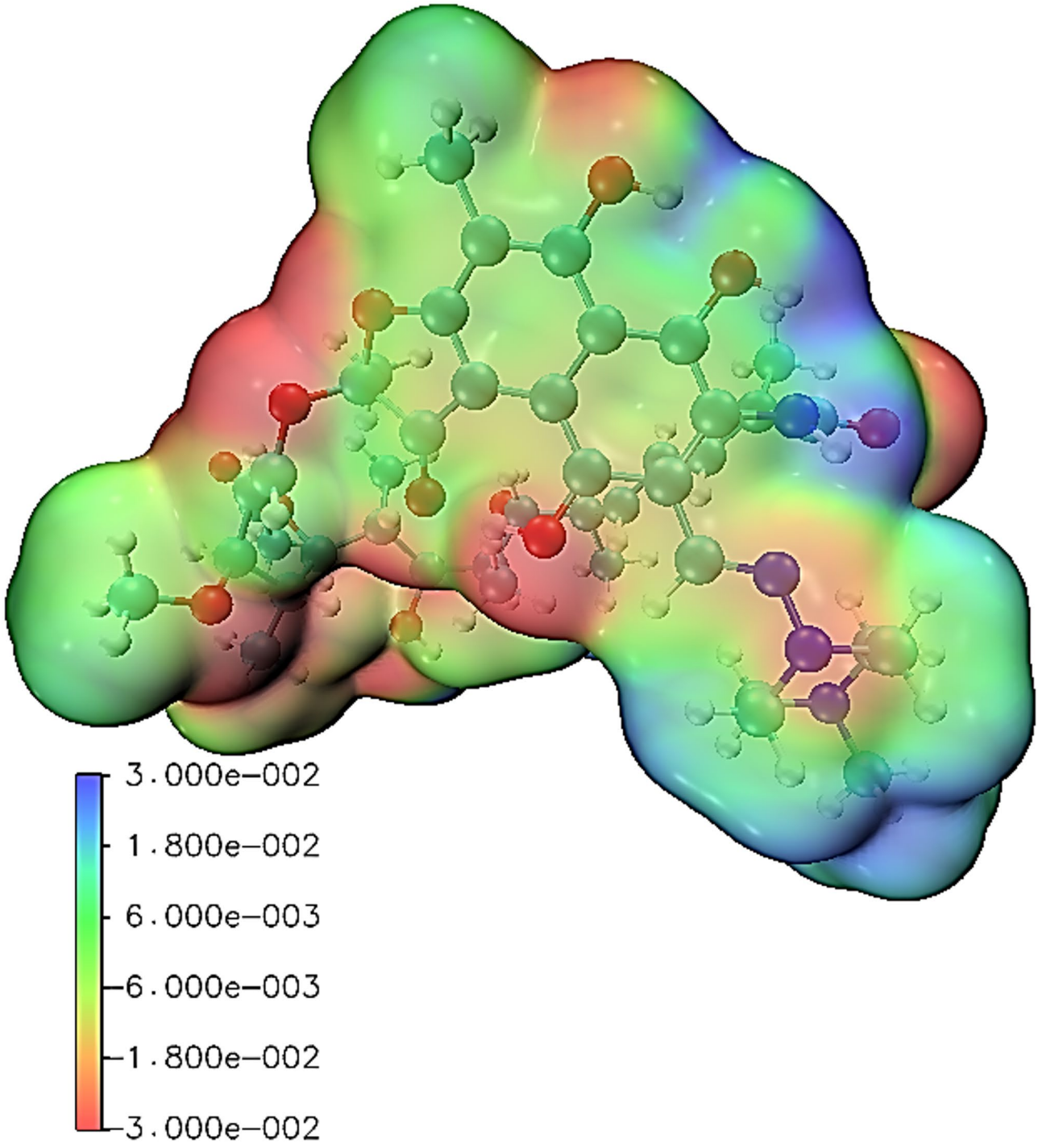

Fig. 7. 3D-colored map of the molecular electrostatic potential of the designed compound.

chosen target protein enzyme, Fumarate hydratase of Mycobacterium tuberculosis (ID:5F92) target protein. To anticipate the inhibition efficiency of the systems under study, several interaction types were constructed. Figure 9 displays the docking results of the designed Rifampicin ligand with significant types of interactions. The ligand's binding energy estimates a value of -36.01 kJ/mol, where the various interactions manifest as non-covalent bonds between the functional group of interest in the ligand under study and a particular location in each amino acid. The most important non-covalent contact that stabilizes the docked complexed conformer is thought to be the traditional hydrogen bond type. The hydrogen bond type found through OH and C = O of the ligand, connected with LYS 290, and TRP 297 in the instance of the 5F92 target. The docked complex stabilization is supported by several beneficial interactions that have been observed, including vdW, alkyl and π-alkyl types. Table 4 presents the most common interaction type through the ligand functional groups and the active site of the target protein.

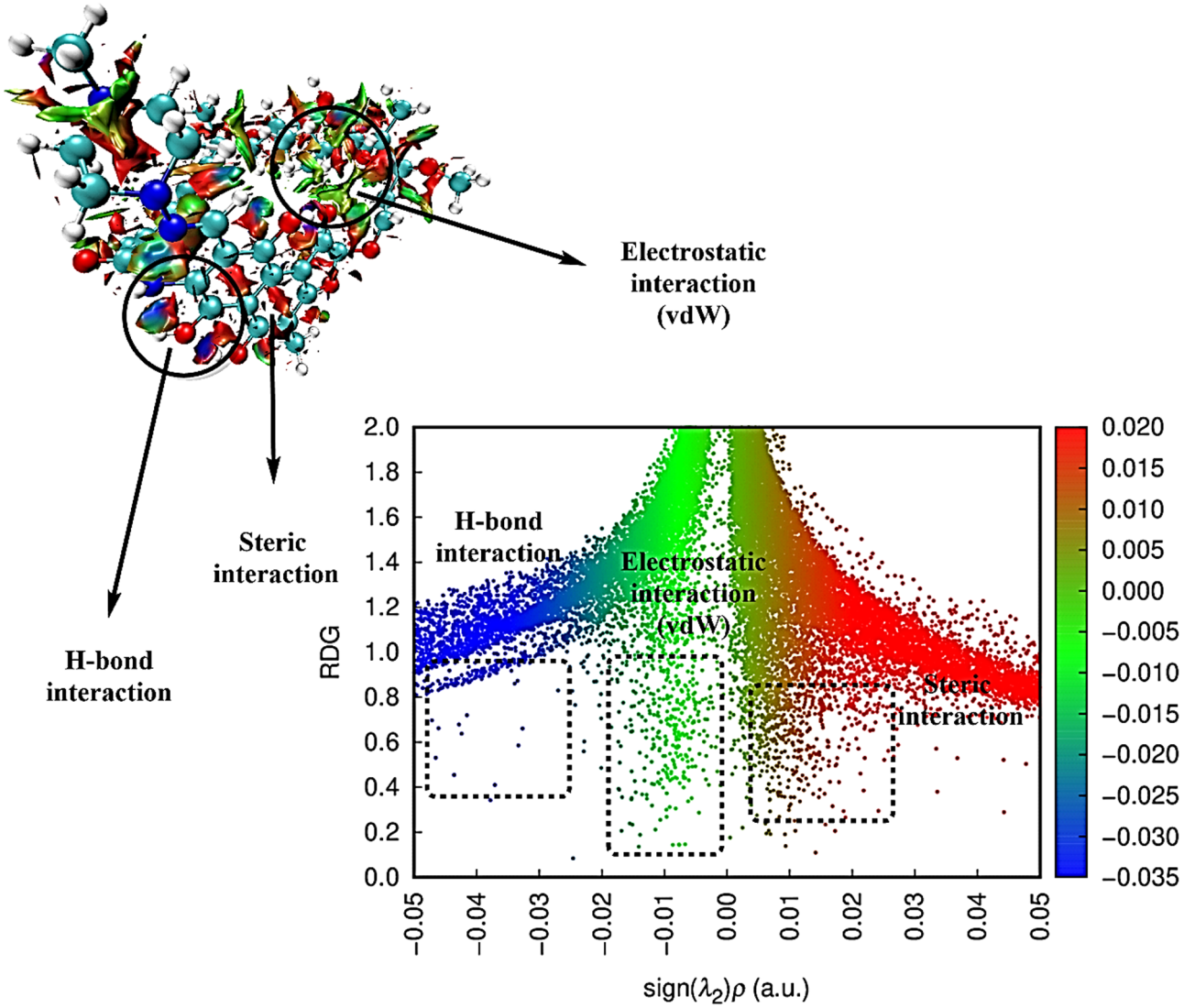

Fig. 8. 3D-NCI map and RDG plot of the designed compound.

Drug likeness and ADMET predictions: Based on five criteria, the Lipinski rule can evaluate the efficacy of the compounds' medicinal qualities: molecular weight < 500 Da, strong lipophilicity (LogP value < 5), H-bond donors < 5, and H-bond acceptors < 10[44]. When a ligand satisfies more than two of these criteria, it may exhibit drug-like characteristics. Rifampicin's drug-likeness characteristics are displayed in Table 5. The ligand's molecular weight was determined to be 822.94 g/mol. It has six hydrogen bond donors and fourteen hydrogen bond acceptors; the examined ligand satisfies these requirements. The molecule's iLog P value (4.335), which is shown to be within the range of less than 5, as anticipated theoretically, indicates excellent permeability across the cell membrane. Although Rifampicin exhibits a high molecular weight (822.94 g/mol) and a topological polar surface area (TPSA) of 220.15 Å², both of which typically suggest poor intestinal absorption, these parameters alone do not fully determine oral bioactivity. In practice, Rifampicin is a well-established orally administered drug, indicating that additional factors can compensate for its unfavorable physicochemical properties. These may include high membrane permeability, active transport via carrier proteins, and formulation strategies that enhance solubility and absorption. Therefore, despite deviations from Lipinski's Rule of Five and Veber's guidelines[45]. Rifampicin demonstrates that oral bioavailability can still be achieved through a combination of favorable ADME characteristics and drug delivery approaches. Also, Rifampicin is known to be orally effective, which implies that it may bypass the limitations predicted by TPSA alone. Possible explanations include its ability to utilize active transport mechanisms, formulation strategies that enhance absorption, or high intrinsic permeability despite its polar nature[46].

Tiny molecules that resemble pharmaceuticals and have great biological activity while being minimally hazardous are the main focus of medical chemistry's drug design, discovery, and modern drug development techniques[47]. ADMET features can be identified using in silico prediction tools, improving activity and toxicity studies' time and resource efficiency[48]. Table 6 displays the pharmacokinetic and lipophilicity metrics (ADMET features). Caco-2 permeability values are typically reported as the logarithm of the permeability coefficient

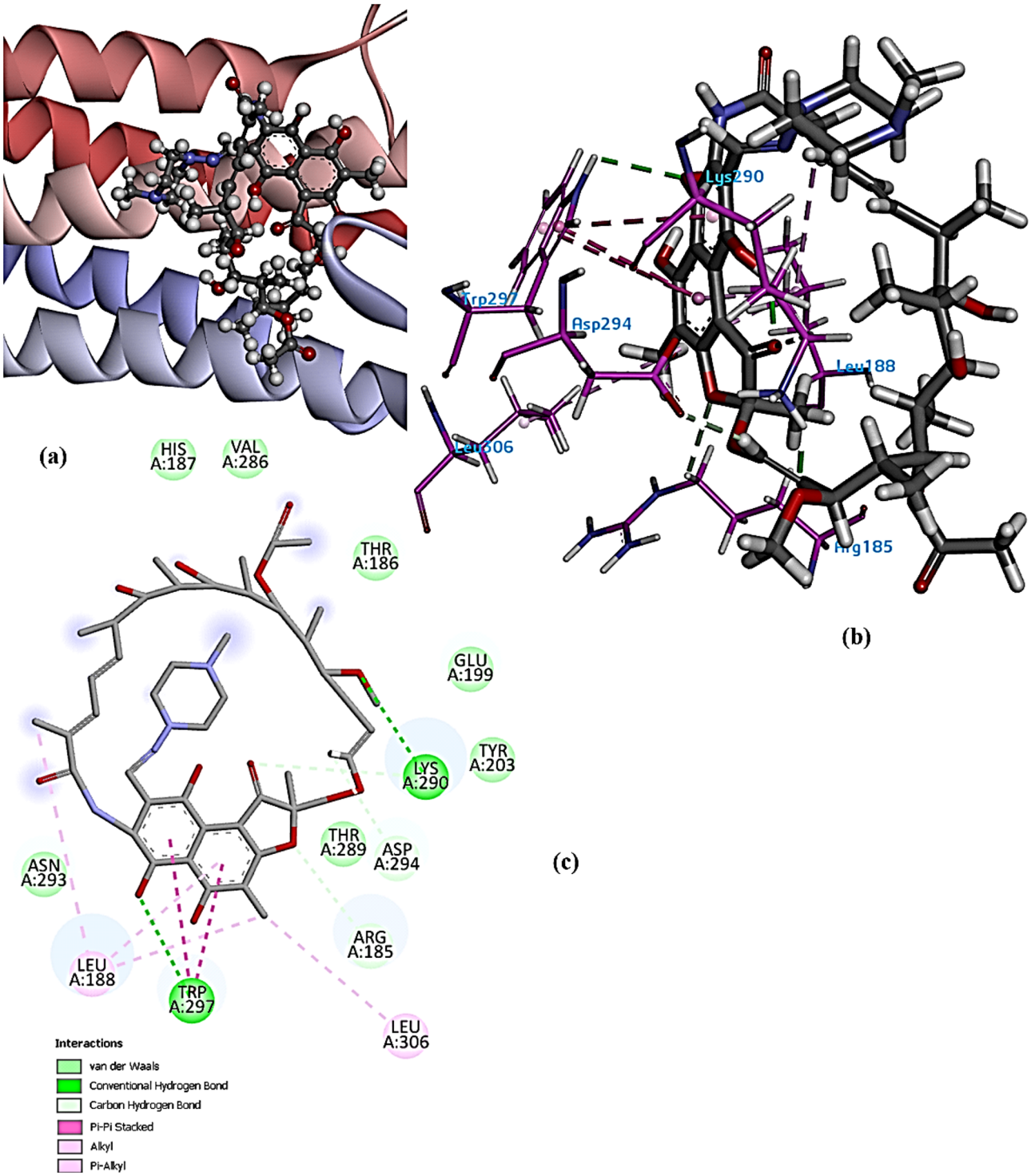

Fig. 9. Molecular docking simulation of Rifampicin against 5F92 target protein, (a) best pose of Rifampicin with 5F92, (b) 3D- reprehensive map of Rifampicin in the predicted active site, (c) 2D-reprehensive map of Rifampicin with the interacted amino acids by several favourable interactions.

(logPapp). A value like −5.246 indicates very low permeability across the Caco-2 cell monolayer, which is commonly used as a model to estimate intestinal absorption of compounds. A Human Intestinal Absorption (HIA) value of 0.942 indicates a high degree of intestinal absorption. This metric is typically expressed as a proportion or percentage of a compound absorbed through the human intestine after oral administration. A P-glycoprotein (Pgp)value of 0.871 indicates a high likelihood that the compound is a substrate for P-glycoprotein (P-gp). The VDss parameter refers to the predicted steady-state volume of distribution (VDss), its value (4.246 L/Kg) provides insight into the extent of a compound's distribution within the body relative to plasma. Metabolic

Model	B.E (kJ/mol)	Ligand interacted part	Residue interacted part	Type of interaction
Rifampicin- Fumarate hydratase of Mycobacterium tuberculosis (5F92)	-36.01	Tetrahydrofuran	ARG 185	Carbon H-bond
		C = O, and phenyl rings	TRP 297	Conventional H-bond, and π-π stacked
		Carbon atoms on the molecule surface	VAL 286	vdW
		OH	LYS 290	Conventional H-bond
		Carbon atoms on the molecule surface	SER 186	vdW
		Carbon atoms on the molecule surface	THR 289	vdW
		Carbon atoms on the molecule surface	ASN 293	vdW
		CHO	ASP 294	Carbon H-bond
		Methyl group	LEU 306	Alkyl interaction
		Carbon atoms on the molecule surface	HIS 187	vdW
		Phenul and methyl groups	LEU 188	Alkyl and π-alkyl
		Carbon atoms on the molecule surface	GLU 199	vdW
		Carbon atoms on the molecule surface	TYR 203	vdW

Table 4. Quantitative content of rifampicin in pharmaceutical preparations determined via the proposed method.

Parameter	Ligand value	Reference value
Hydrogen bond acceptor (HBA)	14	< 10
Hydrogen bond donor (HBD)	6	< 5
Molecular Weight (MW)	822.94 g/mol	< 500
Topological polar surface area (TPSA)	220.15Å²	< 140
LogP	4.335	< 5

Table 5. Drug-likeness descriptors of the predicted rifampicin inhibitor.

Absorption	
Water solubility (mol/L)	-6.188
Caco-2 permeability	-5.246
HIA	0.942
Pgp	0.872
Distribution	
BBB permeability	0.063755
VDss	4.247
Metabolism	
CYP2D6 inhibitor	No
CYP1A2 inhibitor	No
CYP2C19 inhibitor	No
CYP2C9 inhibitor	No
CYP3A4 inhibitor	No
Bioavailability score	0.61
Toxicity	
AMES	0.508
hERG inhibitor	0.712
Skin reaction	0.207
ClinTox	0.343

Table 6. ADMET parameters for the studied compound.

factors can be used to assess a substance's ability to block five isoenzymes associated with cytochrome P450, a primary drug-metabolizing enzyme (CYP1A2, CYP2C19, CYP2C9, CYP2D6, and CYP3A4). CPY is used to create therapeutic effects and prevent them from working. For toxicity and other adverse drug interactions, this characteristic is crucial[49]. These kinds of drug-metabolizing enzymes are unaffected by the anticipated drug's strong ligand. A probable physicochemical property that qualifies the chosen target molecule for oral

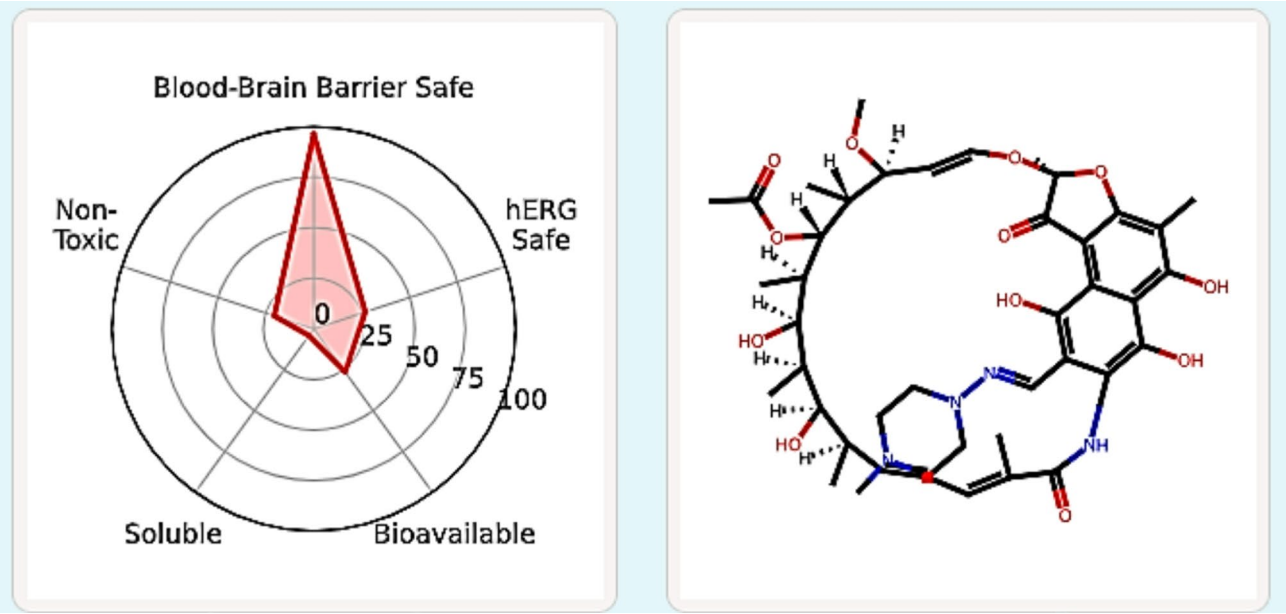

Fig. 10. Radar model of the predicted Rifampicin inhibitor.

bioavailability was exported. The AMES test evaluates a compound's potential to cause mutagenicity, i.e., whether it induces genetic mutations that could lead to cancer. The AMES value of 0.508 suggests a borderline case, leaning slightly toward potential mutagenicity. ClinTox is one of the key parameters in the ADMET (Absorption, Distribution, Metabolism, Excretion, and Toxicity) profiling of a drug. It specifically refers to clinical toxicity, which assesses the potential toxic effects of a drug in humans. The value of ClinTox for the designed compound (0.343) suggests a moderate to low risk of clinical toxicity. Creating a radar plot for the predicted Rifampicin inhibitor involves visualizing key ADMET properties or molecular features of the compound. Radar plots (or spider charts) are excellent tools for comparing multiple attributes. Figure 10 estimates the radar plot for the predicted Rifampicin inhibitor. It visualizes the normalized ADMET parameters, highlighting the relative strengths and weaknesses of the compound.

Conclusion

The results of this study indicated that, the proposed method simple, direct, and easily applicable to be used for the determination of Rifampicin in its pure and/ or pharmaceutical forms. Comparing the results of this study to the results of the same method was rather difficult due to the lack data in the existing literature. Although there was other research that applied this method, but for different drugs, this study provides another step in the methods of determination of Rifampicin. Compared to the conditions utilized in the previously described methods, the developed approach use simpler conditions. Additionally, this technique decrease waste, prevent chemical derivatization, heating, or extraction; its also improve operator safety. The absence of matrix source interference is another benefit, making it appropriate for routine determinations of rifampicin in pure form and preparations for evaluating the stability of its formulation. The docking simulations reveal critical binding residues and interaction energies, emphasizing rifampicin's potential inhibitory action and supporting its pharmacological relevance. The integrated DFT and docking approach highlights rifampicin's electronic characteristics and binding efficacy, providing a framework for rational drug design and optimization. MEP analysis demonstrated the highly electronic rich sites mostly present on oxygen atoms. The other electron poor sites significantly appear around the H-bond interaction centers. RDG analysis confirmed the presence of strong H-bonds that control the stability of the molecule. Molecular docking simulation revealed a potent affinity towards 5F92 complexation with binding energy value of -36.01 kcal/mol. Rifampicin demonstrates significant oral bioavailability, facilitated by favorable absorption characteristics. Its distribution profile indicates significant tissue penetration, including effective traversal into target sites such as macrophages and the blood-brain barrier. Toxicity predictions show rifampicin has a tolerable safety margin, although hepatotoxicity and hypersensitivity reactions are documented in certain populations. Overall, Rifampicin exhibits a balanced ADMET profile, supporting its extensive use in treating tuberculosis and other bacterial infections. This analysis underlines its therapeutic potential while highlighting areas for cautious clinical monitoring to mitigate adverse effects and optimize patient outcomes.

Data availability

Data is provided within the manuscript .

Received: 24 March 2025; Accepted: 10 June 2025
Published online: 11 July 2025

References

1. The British Pharmacopoeia. London Stationary Office 2022, II-820.
2. Fairuz, H. A. T. & Bushra, K. Q. Molecular analysis of rifampicin resistance conferring mutations in Mycobacterium tuberculosis. *Baghdad Sci. J.* **17**(2), 444–451 (2020).
3. Dalal, S. A. et al. Genotypic assessment of drug-resistant tuberculosis in Baghdad and other Iraqi provinces using low-cost and low-density DNA microarrays. *J. Med. Microbiol.* **65**(2), 114–122 (2015).
4. Lubna, A. S., Alaa, A. A. & Muayad, A. S. Formulation of rifampicin suspension. *Iraqi J. Pharm. Sci.* **15**(2), 1–7 (2006).
5. Sabrei, D. A. Study the Effect of Rifampicin in the Level of Thyroid's Gland Hormones and Thyroid - Stimulating Hormone in Rabbits. *IHJPAS*, **22**(3). (2009).
6. Tamara, W. K. & Kais, K. G. Effect the natural efflux pump inhibitor (Berberine) in multidrug resistant Kleibsiella pneumoniae isolated from urinary tract infections in several Baghdad hospitals. *Egypt. J. Hosp. Med.* **89**(2), 6882–6888 (2022).
7. Anwar, K. A., Khaled, A. A. & Ahmed, M. A. Resistance of anti-tuberculosis drugs among pulmonary tuberculosis patients in Yemen. *J. Fac. Med. Baghdad*. **55**(3), 250–253 (2013).
8. Rajendra, M. K. & Foram, N. P. Analytical methods practiced to quantitation of rifampicin: A captious survey. *Curr. Pharm. Anal.* **17**(8), 983–999 (2021).
9. Irena, Y. B., Mayar, L. G., Luis, M. & Jean, L. D. Chromatographic methods for the determination of rifampicin, isoniazid, pyrazinamide, ethambutol, and main metabolites in biological samples: A review. *Crit. Rev. Anal. Chem.* **29**, 1–16 (2022).
10. Nada, H. B., Syed, N. A. & Muhammad, M. H. Development and validation of HPLC method for the determination of rifampicin in human plasma. *Saudi J. Med. Pharm. Sci.* **5**(7), 654–658 (2019).
11. Paula, R. C. et al. Development and validation of an HPLC method for simultaneous determination of rifampicin, isoniazid, pyrazinamide, and ethambutol hydrochloride in pharmaceutical formulations. *Journal AOAC International*, **98**(5). (2015).
12. Salem, A. A., Mossa, H. A. & Barsoum, B. N. Quantitative determinations of Levofloxacin and rifampicin in pharmaceutical and urine samples using nuclear magnetic resonance spectroscopy. *Spectrochim Acta Mol. Biomol. Spectrosc.* **62**(1–3), 466–472 (2005).
13. Yong, W., YongNian, N. & Serge, K. Simultaneous kinetic spectrophotometric determination of Norfloxacin and rifampicin in pharmaceutical formulation and human urine samples by use of chemometrics approaches. *Sci. China Ser. B: Chem.* **51**, 776–785 (2008).
14. Nouri, F. & Alassaf, N. Partial least squares method for the multicomponent analysis of antibacterial mixture. *Methods Objects Chem. Anal.* **18**(2), 92–100. https://doi.org/10.17721/moca.2023.92-100 (2023).
15. Zhengqing, L. et al. Determination of rifampicin based on fluorescence quenching of GSH capped cdte/zns QDs. *J. Lumin.* **132**, 2484–2488 (2012).
16. Shewiyo, D. H. et al. Optimization of a reversed-phase-high-performance thin-layer chromatography method for the separation of isoniazid, ethambutol, rifampicin and Pyrazinamide in fixed-dose combination antituberculosis tablets. *J. Chromatogr. A.* **1260**, 232–238 (2012).
17. Indorica, S. & Muhammad, H. Z. Evaluation of the effect of temperature on the stability and antimicrobial activity of rifampicin Quinone. *Journal Pharm. Biomedical Analysis*, 197. (2021).
18. Žane, T. R. et al. Fast and Simple LC-MS/MS Method for Rifampicin Quantification in Human Plasma. *International Journal of Analytical Chemistry*, Volume 2019. (2019).
19. Swamy, N. & Basavaiah, K. Spectrophotometric determination of rifampicin in bulk drug and pharmaceutical formulations based on redox and complexation reactions. *J. Appl. Spectrosc.* **84**(4), 694–703 (2017).
20. Sourav, K., Sampurna, P., Suddhasattya, D., Sudip, K. M. & Saptarshy, S. Simultaneous spectrophotometric Estimation of rifampicin, Isoniazid and Pyrazinamide in their pharmaceutical dosage form. *Asian J. Res. Chem.* **13**(2), 117–122 (2020).
21. Bhoyar, V., Belgamwar, V. S. & Trivedi, S. Simultaneous determination and validation of Anti-Tubercular drugs in simulated lungs alveolar macrophages fluid by Ultraviolet-Visible spectrophotometric method. *J. Appl. Spectrosc.* **89**, 892–897 (2022).
22. Farah, N., Nahla, A. & Alassaf Partial least squares method for the multicomponent analysis of antibacterial mixture. *Methods Objects Chem. Anal.* **18**(2), 92–100 (2023).
23. Validation of analytical. procedures: text and methodology, in: International Conference on Harmonization (ICH), Q2(R1), IFPMA, Geneva, Switzerland, (2005).
24. Parr, R. G. & Yang, W. *Density Functional Theory of Atoms and Molecules* (Oxford University Press, 1989).
25. Ibraheem, H., Al-Majedy, Y., Issa, A. A. & Yousif, E. Photostabilization, thermodynamic and theoretical studies of polystyrene by some 2-amino pyridine. *Trends Sci.* **21**, 7374. https://doi.org/10.48048/tis.2024.7374 (2023).
26. Frisch, M. J. et al. *Gaussian 09, Revision A.02* (Gaussian, Inc., 2016).
27. Zhurko, G. & Zhurko, D. ChemCraft 1.8, (2005). http://www.chemcraftprog.com.
28. Humphrey, W., Dalke, A. & Schulten, K. `VMD – Visual molecular dynamics'. *J. Molec Graphics*. **14**(1), 33–38 (1996).
29. Lu, T., Chen, F. & Multiwfn A multifunctional wavefunction analyzer. *J. Comput. Chem.* **33**(5), 580–592. https://doi.org/10.1002/jcc.22885 (2011).
30. Yu, J., Su, N. Q. & Yang, W. Describing chemical reactivity with frontier molecular orbitalets. *JACS Au*. **2**(6), 1383–1394 (2022).
31. Waleed, A. et al. Adsorption locator behavior of Polycyclic-Carbon based systems: computational optical and dynamic properties. *Russ J. Gen. Chem.* **94**, 2676–2688. https://doi.org/10.1134/S107036322410013X (2024).
32. Rezvan, V. H. Molecular structure, HOMO–LUMO, and NLO studies of some Quinoxaline 1, 4-dioxide derivatives: computational (HF and DFT) analysis. *Results Chem.* **7**, 101437 (2024).
33. Ibraheem, H. H. et al. Insights into the pharmaceutical properties and in Silico study of novel hydrazone derivatives. *Sci. Rep.* **14**, 1–18. https://doi.org/10.1038/s41598-024-81555-z (2024).
34. Kasbekar, M. et al. Selective Small Molecule Inhibitor of the Mycobacterium Tuberculosis Fumarate Hydratase Reveals an Allosteric Regulatory Site. Proceedings of the National Academy of Sciences 113(27), 7503–7508. (2016). https://doi.org/10.1073/pnas.1600630113
35. Issa, A. A. et al. Nanocluster-Based computational creation of a potential carrier for chemotherapeutic antibacterial drugs. *J. Inorg. Organomet. Polym. Mater.* 1–16. https://doi.org/10.1007/s10904-024-03116-1 (2024).
36. El, S., Khalil, T. E. & Elbadawy, H. A. Rational and experimental investigation of antihypotensive Midodrine-Fe(III) complex: synthesis, spectroscopy, DFT, biological activity and molecular Docking. *J. Mol. Struct.* 138421–138421. https://doi.org/10.1016/j.molstruc.2024.138421 (2024).
37. Ruba, F. A. & Bahaa, M. A. High performance liquid chromatographic and area under curve spectrophotometric methods for Estimation of cefixime in pure and marketed formulation: A comparative study. *Res J. Chem. Environ*, **24**(6). (2020).
38. Yuri, K., Yuri, K. & Andrey, S. Comparison of integration rules in the case of very narrow chromatographic peaks. *Chemometr. Intell. Lab. Syst.* **179**, 22–30 (2018).
39. Azeez, Y. H., Kareem, R. O., Qader, A. F., Omer, R. A. & Ahmed, L. O. Spectroscopic characteristics, stability, reactivity, and corrosion Inhibition of AHPE-dop compounds incorporating (B, fe, ga, Ti): a DFT investigation. *Next Mater.* **3**, 100184 (2024).
40. Abdelrehim, E. M. & El-Sayed, D. S. A new synthesis of Poly heterocyclic compounds containing [1,2,4]Triazolo and [1,2,3,4] Tetrazolo moieties and their DFT study as expected Anti-Cancer reagents. *Curr. Org. Synth.* **17**(3), 211–223. https://doi.org/10.2174/1570179417666200226092516 (2020).
41. Hossain, M. A., Sultana, S., Islam, M. M., Akhter, S., Nur, F., Majabin, F., … Kawsar,S. M. (2023). DFT-Based Chemical Reactivity Descriptors, Pharmacokinetics and Molecular Docking Studies of Thymidine Derivatives. Computational Chemistry, 11(4), 81–103.

42. Sagaama, A., Issaoui, N., Bardak, F., Al-Dossary, O., Kazachenko, A. S., Karrouchi,K., … Wojcik, M. J. (2022). Non covalent interactions analysis and spectroscopic characterization combined with molecular docking study of N′-(4-Methoxybenzylidene)-5-phenyl-1H-pyrazole-3-carbohydrazide.Journal of King Saud University-Science, 34(2), 101778.
43. Issa, A. A., Kamel, M. D. & El-Sayed, D. S. Depicted simulation model for removal of second-generation antipsychotic drugs adsorbed on Zn-MOF: adsorption locator assessment. *J. Mol. Model.* **30**, 106. https://doi.org/10.1007/s00894-024-05896-2 (2024).
44. Mahmood, W. K., Dakhal, G. Y., Younus, D., Issa, A. A. & El-Sayed, D. S. Comparative properties of ZnO modified au/fe nanocomposite: electronic, dynamic, and locator annealing investigation. *J. Mol. Model.* **30**, 165. https://doi.org/10.1007/s00894-024-05956-7 (2024).
45. Matsson, P., Doak, B. C., Over, B. & Kihlberg, J. Cell permeability beyond the rule of 5. *Adv. Drug Deliv. Rev.* **101**, 42–61. https://doi.org/10.1016/j.addr.2016.03.013 (2016).
46. Marsot, A. et al. Evaluation of current dosing guidance for oral rifampicin treatment in adult patients with osteoarticular infections. *Br. J. Clin. Pharmacol.* **86**(11), 2319–2324. https://doi.org/10.1111/bcp.14319 (2020). Epub 2020 May 13. PMID: 32330996; PMCID: PMC7576626.
47. Ferreira, L. L. & Andricopulo, A. D. ADMET modeling approaches in drug discovery. *Drug Discov Today*. **24**(5), 1157–1165 (2019).
48. Mani, N., Nicksonsebastin, D. & Prasath, M. Quantum computational, spectroscopic, ADMET, molecular Docking and dynamics simulation revealing the Inhibition of psoralidin against anti-tuberculosis. *Chem. Phys. Impact*. **7**, 100292 (2023).
49. Zhao, M. et al. Cytochrome P450 enzymes and drug metabolism in humans. *Int. J. Mol. Sci.* **22**(23), 12808. https://doi.org/10.3390/ijms222312808 (2021). PMID: 34884615; PMCID: PMC8657965.

Acknowledgements

The authors appreciated the University of Baghdad –Iraq, and University of technology- Iraq, for the logistic support of this work. Also, the authors extend their appreciation to the researchers supporting project number (RSPD2025R971), King Saud University, Riyadh, Saudi Arabia, for funding this study.

Author contributions

N. A. A., A. S. H., and M. S. J.: Writing Original draft, Methodology, Investigation and Formal analysis. N. A. A., and A. S. H., S. Gh., A. A. S. : Main Concept, Data interpretation, and supervision. N. A. A., A.S. H., and M. S. J.: Writing-review and editing, Visualization, and Data curation. All authors reviewed the manuscript.

Declarations

Competing interests

The authors declare no competing interests.

Conflict of interest

The authors declare no competing interests.

Additional information

Correspondence and requests for materials should be addressed to M.S.J. or A.A.S.

Reprints and permissions information is available at www.nature.com/reprints.

Publisher's note Springer Nature remains neutral with regard to jurisdictional claims in published maps and institutional affiliations.